Bulk and surface spin conductivity in topological insulators with hexagonal warping

R. S. Akzyanov and A. L. Rakhmanov
Moscow Institute of Physics and Technology, Dolgoprudny, Moscow Region 141700, Russia;
Institute for Theoretical and Applied Electrodynamics, Russian Academy of Sciences, Moscow 125412, Russia;
Dukhov Research Institute of Automatics, Moscow 127055, Russia;
and P. N. Lebedev Physics Institute, Moscow 119991, Russia

(Received 28 June 2018; published 23 January 2019)

We investigate the spin conductivity of topological insulators taking into account both the surface and quasi-two-dimensional bulk states. We apply a low-energy expansion of the Hamiltonian up to the third order in momentum and take into account the vertex corrections arising due to the short-range disorder. Hexagonal warping gives rise to the additional anisotropic components in the spin conductivity tensor. Typically, the isotropic part of the spin conductivity is larger than the anisotropic one. The helical regime for the bulk states, in which the electrons in the Fermi level have the same projection of the spin on the direction of momentum, have been studied in more detail. In this regime, a substantial increase of the spin conductivity contribution from the bulk states at the Fermi level is observed. We find that the bulk spin conductivity is insensitive to disorder if Rashba spin-orbit coupling is larger than disorder strength, otherwise, it is strongly suppressed. The contribution to the spin conductivity from the surface states is almost independent of the chemical potential, robust to disorder and its value is comparable to the spin conductivity contribution from the bulk states per layer. The obtained results are in agreement with experimental data.

DOI: 10.1103/PhysRevB.99.045436

I. INTRODUCTION

Topologically protected surface states form a Dirac cone in the electronic spectrum of the topological insulators (TIs) [1]. The electron dispersion near Dirac points is linear. However, a hexagonal warping of the Dirac cone arises when we take into account the next-order terms in the momentum expansion of corresponding Hamiltonian of the TIs with the hexagonal lattices, such as Bi_2Te_3 [2] and Bi_2Se_3 [3]. The hexagonal warping influences not only the surface states but also quasi-two-dimensional bulk states in these systems. Effects of the hexagonal warping on the electronic properties of the TI have been studied extensively [4–7]. In our recent paper [8], we find that the presence of the hexagonal warping significantly affects the charge conductivity of the TI. In particular, it gives rise to the anisotropic anomalous in-plane magnetoresistance. Hexagonal warping also affects the quantum anomalous Hall effect and anomalous out-of-plane magnetoresistance.

A remarkable feature of the TIs is the existence of high spin conductivity in the absence of magnetic field, which is associated with an intrinsic spin Hall effect [9]. This effect has been first predicted in Rashba [10] and Dresselhaus [11] spin-orbit coupled materials. However, the intrinsic spin Hall effect in such materials is weak due to short-range disorder (from a theoretical point of view, due to vertex corrections caused by this disorder) [12,13].

A change of direction of the magnetization in the magnetic material by a spin current is referred to as spin-transfer torque (STT) [14]. The STT is closely related to the spin conductivity [15]. This effect can be used for the design of the fast and low dissipative magnetic memory [16]. Recent experiments reveal that STT in the TIs is by orders of magnitude larger than for any other material, which is a sign of a substantial spin conductivity in TIs [17–20]. Experimental study of the STT in the TIs demonstrates some intriguing features. Both the in-plane and out-of-plane STT exist in the system, and the value of these effects is of the same order, which is unexpected from the spin-momentum locking argument [17]. Moreover, the sign of the spin conductivity may be different in different samples of the same material [21]. Spin conductivity in the TI is tuned by chemical potential and obeys a particle-hole asymmetry [19,22]. Also, spin conductivity is suppressed in the bulk-insulating regime [22]. It has been speculated that the large spin currents arise in the TIs due to the existence of the topologically protected surface states [23–25]. However, in the other papers it is complained that the spin current in the TI mainly comes from the bulk states [20,26]. Also, recent theoretical paper reveals that the contribution of bulk states should be taken into account to model the experiments on the spin-orbit torque in the TI [27]. A rather different approach is to measure bilinear magnetoelectric resistance [28,29] that is believed to be proportional to the spin current [30]. This resistance scales linearly with applied electric field and can be used to determine spin-orbit torques [31].

In general, the spin conductivity includes both contributions from the states at the Fermi surface and from all filled states [32,33]. While the contribution to the spin conductivity from the filled states can be calculated in a clean limit [10,11], it is vital to treat the disorder correctly to describe the contribution from the states at the Fermi level [12,13].

An unexpectedly small number of theoretical works are devoted to the spin conductivity in TIs. Recent DFT calculations of the contribution to the spin conductivity from the filled states show that quite large spin currents can exist in

Bi_xSb_{1-x} and the value of the spin conductivity can be tuned by the chemical potential variation [34]. In Ref. [35], the spin conductivity of the surface states in a thin film of TI with a cubic lattice has been studied neglecting the vertex corrections. The authors concluded that the dependence of the surface spin conductivity on the disorder and chemical potential is small. The spin conductivity in another Dirac material, graphene, attracted much more attention [36–38]. Provided the spin-orbit interaction is induced in graphene, quite reasonable spin currents can be obtained in it. Recent calculations also show that large spin currents can be induced in Weyl semimetal, another Dirac material with large spin-orbit interaction [39].

We study the spin conductivity of the surface and bulk states in the TI in a low-energy approximation with taking into account the hexagonal warping. Both contributions from the filled states and from the states at the Fermi surface are considered. We apply the Kubo formalism accounting the vertex corrections to the velocity operators arising due to the short-range disorder. We show that the presence of the hexagonal warping leads to the additional anisotropic terms in the spin conductivity. We get that the spin conductivity is robust against disorder. The spin conductivity of the surface states is comparable with the spin conductivity of the bulk states per layer. The obtained results are consistent with the experimental data.

The paper is organized as follows. In Sec. II we analyze the Hamiltonian describing the surface and bulk states in the TI. In Sec. III we introduce disorder and in Sec. IV calculate the vertex corrections to the velocity operator. In Sec. V we study the contribution to the bulk and surface spin conductivity from the states at the Fermi level. In Sec. VI we consider the contribution to the spin conductivity from the filled states. We estimate the values of the characteristic for TIs parameters in Sec. VII. In Sec. VIII we discuss the obtained results and compare them with the experiments and numerical calculations.

II. MODEL

We consider a two-dimensional time-reversal Hamiltonian with C_{3v} symmetry. This symmetry consists of a threefold rotation C_3 around z axis and a mirror operation $x \to -x$. The low-energy Hamiltonian with such symmetries is written as [2,40] ($\hbar = 1$)

$$\hat{H} = r\left(k_x^2 + k_y^2\right) + \mu + \alpha_{Rk}(k_x\sigma_y - k_y\sigma_x) + \lambda k_x\left(k_x^2 - 3k_y^2\right)\sigma_z,$$
$$\alpha_{Rk} = \alpha_R\left[1 + s\left(k_x^2 + k_y^2\right)\right], \quad (1)$$

where $\sigma = (\sigma_x, \sigma_y, \sigma_z)$ are the Pauli matrices acting in spin space, μ is the chemical potential, α_R is the value of Rashba coupling (it is proportional to spin splitting of the bulk states and equal to the Fermi velocity for the surface states), $r = 1/(2m)$ is the inverse mass term, s characterizes the next-order correction in momentum to α_R, $k_x = k\cos\phi$, and $k_y = k\sin\phi$ are the in-plane momentum components, λ is the hexagonal warping coefficient. The term in the Hamiltonian responsible for the hexagonal warping can be rewritten as $\lambda k_x(k_x^2 - 3k_y^2) = \lambda k^3\cos 3\phi$ and the Hamiltonian is invariant under rotation on the angle $\phi = 2\pi/3$. The form of the Hamiltonian is fixed by the symmetries. Such Hamiltonian can describe the surface and quasi-two-dimensional bulk states in the TI, such as Bi_2Se_3 and Bi_2Te_3 [40]. Also, this Hamiltonian can also describe the quasi-two-dimensional states of BiTeI [41]. This Hamiltonian neglects complex multiorbital structure of the TI states and should be considered as a minimal model that preserves given symmetries.

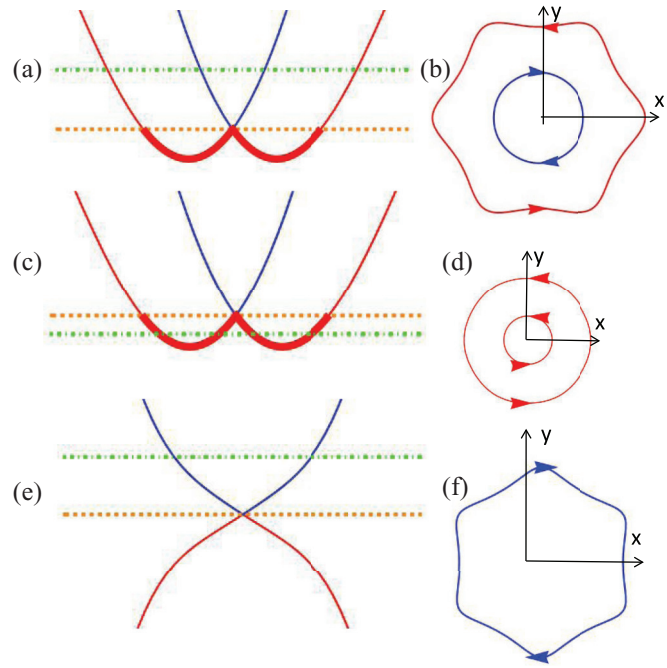

FIG. 1. Energy spectrum, Eq. (2), and corresponding Fermi surface for different values of parameters. Spin direction of the states in the Fermi level is shown by arrows. (a)–(d) illustrate the spectrum and the Fermi surface for the bulk states at $s = 0$ and $\lambda\alpha_R/r^2 = 0.2$; $r\mu/\alpha_R^2 = -2$ in (a) and (b), $r\mu/\alpha_R = 0.2$ in (c) and (d). Bold lines in (a) and (c) indicate the helical regime. (e) and (f) illustrate the spectrum and the Fermi surface for the surface states at $s\alpha_R^2/r^2 = 10$, $\lambda/s\alpha_R = 0.2$, and $r\mu/\alpha_R = 0.2$. Orange dashed lines indicate zero of the chemical potential and green dot-dashed lines show the chemical potential.

The spectrum of the Hamiltonian (1) is given by

$$E_\pm = \mu + rk^2 \pm \sqrt{\alpha_{Rk}^2 k^2 + \lambda^2 k^6\cos^2 3\phi}. \quad (2)$$

If we measure the energy in terms of α_R^2/r then the chemical potential, the next-order correction to the spin-orbit coupling, and the hexagonal warping are conveniently characterized by the dimensionless values $r\mu/\alpha_R^2$, $s\alpha_R^2/r^2$, and $\lambda\alpha_R/r^2$, respectively.

Energy spectrum (2) is shown in Fig. 1 for different set of parameters characteristic of the bulk, Figs. 1(a) and 1(c), and surface, Fig. 1(e), states. A key feature of the surface states in the TI is the existence of a robust Dirac cone, which is the case if $s\alpha_R^2/r^2$ is sufficiently large, Fig. 1(e). The corresponding Fermi surface has a characteristic form of a snowflake, Fig. 1(f). The bulk states corresponds to smaller values of $s\alpha_R^2/r^2$, Figs. 1(a) and 1(c). In the latter case, the spectrum has an appearance characteristic of a two-dimensional electron gas with bands split due to the Rashba spin-orbit interaction.

Corresponding Fermi surfaces with two pockets are shown in Figs. 1(b) and 1(d) for different values of the chemical potential. Note, that this model describes well ARPES data for the surface and bulk states in the TIs [2,3,40].

We obtain from Eq. (2) that the robust Dirac cone exists when $s\alpha_R^2/r^2 > 1/3$. For $\alpha_R(s\alpha_R+\lambda)/r^2 < 1/4$, two spin split bands emerge in the system as it is expected for the Rashba electron gas. Therefore, we can formally to write down that

$$\begin{aligned} \alpha_R(s\alpha_R+\lambda)/r^2 &< 1/4, \quad \text{bulk states}, \\ \alpha_R^2 s/r^2 &> 1/3, \quad \text{surface states}. \end{aligned} \tag{3}$$

In the case of the bulk states, the function $E_-(k)$ decreases at large k and a proper momentum cutoff k_{cut} must be introduced to avoid arising fake Fermi surface pockets at large momentum. We define cutoff momentum as $k_{\text{cut}} = r/(2s\alpha_R + 2\lambda)$.

We can calculate average spin projection of electrons as $\langle S_\alpha\rangle_\pm = \langle u_\pm|S_\alpha|u_\pm\rangle$, where S_α is the spin operator and $u_\pm$ are eigenfunctions corresponding to the bands $E_\pm$. The in-plane spin polarization component is schematically shown in Figs. 1(b), 1(d), and 1(f). The calculated spin polarization lies in the (x, y) plane if we neglect the hexagonal warping. We see that each band can be characterized by helicity, that is, the sign of the projection of the spin on the direction of momentum. The z component of the spin polarization arises if we take into account that $\lambda \neq 0$. If $\mu < 0$ the bulk states have two split Fermi surfaces with different helicity, see Fig. 1(b). In the case of $\mu > 0$ two Fermi surfaces have the same helicity, see Fig. 1(d), so, we call this regime for the bulk states as helical. Surface states are helical in any case, see Fig. 1(f).

In general, the spin conductivity can be presented as a sum of three terms [32,33]

$$\sigma_{\alpha\beta}^{\gamma} = \sigma_{\alpha\beta}^{\gamma I} + \sigma_{\alpha\beta}^{\gamma II} + \sigma_{\alpha\beta}^{\gamma III}, \tag{4}$$

where the first two items correspond to a contribution from the states at the Fermi surface and the third one from the filled states. Here α and β denote the in-plane coordinates x and y, respectively, and γ denotes the spin projection.

At zero temperature $\sigma_{\alpha\beta}^{\gamma I}$ and $\sigma_{\alpha\beta}^{\gamma II}$ can be written in the form [12,32]

$$\sigma_{\alpha\beta}^{\gamma I} = \frac{e}{4\pi}\int \frac{d^2k}{(2\pi)^2}\text{Tr}\big[j_\alpha^\gamma\, G^+\, V_\beta\, G^-\big], \tag{5}$$

$$\sigma_{\alpha\beta}^{\gamma II} = -\frac{e}{8\pi}\int \frac{d^2k}{(2\pi)^2}\text{Tr}\big[j_\alpha^\gamma\, G^+\, V_\beta\, G^+ + j_\alpha^\gamma\, G^-\, V_\beta\, G^-\big]. \tag{6}$$

Here $j_\alpha^\gamma = \{\sigma_\gamma, v_\alpha\}/4$, $v_\alpha = \partial H/\partial k_\alpha$ is the is the velocity operator, V_α is the velocity operator with vertex corrections, $\{,\}$ means the anticommutator, and $G^\pm$ are the retarded and advanced disorder averaged Green's functions, which will be specified in the next section.

The contribution to the spin conductivity from the filled states is [10,42]

$$\sigma_{\alpha\beta}^{\gamma III} = e\sum_{\mathbf{k},n\neq n'}(f_{n\mathbf{k}} - f_{n'\mathbf{k}}) \times \frac{\text{Im}\langle u_{n'\mathbf{k}}|j_\alpha^\gamma|u_{n\mathbf{k}}\rangle\langle u_{n\mathbf{k}}|v_\beta|u_{n'\mathbf{k}}\rangle}{\Gamma^2 + (E_{n\mathbf{k}} - E_{n'\mathbf{k}})^2}. \tag{7}$$

Here $E_{n\mathbf{k}}$ is the energy of an electron in the nth band with the momentum $\mathbf{k}$, $u_{n\mathbf{k}}$ is the corresponding Bloch vector, $\hat{H}u_{n\mathbf{k}} = E_{n\mathbf{k}}u_{n\mathbf{k}}$, $f_{n\mathbf{k}}$ is the Fermi distribution function corresponding to $E_{n\mathbf{k}}$ (which is the Heaviside step function in the considered case of zero temperature), $\langle\ldots\rangle$ means impurity averaged, and Γ is the disorder parameter or scattering rate. The latter will be also specified in the next section.

III. DISORDER

We will describe disorder by a potential of randomly distributed point defects $V_{\text{imp}} = u_0\sum_i \delta(\mathbf{r} - \mathbf{R}_j)$, where $\delta(\mathbf{r})$ is the Dirac δ function, $\mathbf{R}_j$ are positions of the randomly distributed pointlike impurities with the local potential u_0 and concentration n_i. We assume that the disorder is Gaussian, that is, $\langle V_{\text{imp}}\rangle = 0$ and $\langle V_{\text{imp}}(\mathbf{r}_1)V_{imp}(\mathbf{r}_2)\rangle = n_i u_0^2\delta(\mathbf{r}_1 - \mathbf{r}_2)$.

In the self-consistent Born approximation (SCBA), the impurity-averaged Green's functions can be calculated as

$$G^\pm = G_0^\pm + G_0^\pm\Sigma^\pm G^\pm, \tag{8}$$

where $G_0^\pm$ are bare Green's functions of the Hamiltonian (1)

$$G_0^\pm = \frac{\mu + rk^2 \pm i0 - \alpha_{Rk}(k_x\sigma_y - k_y\sigma_x) - \lambda k^3\cos 3\phi\,\sigma_z}{[\mu + rk^2 \pm i0]^2 - \alpha_{Rk}^2k^2 - (\lambda k^3\cos 3\phi)^2} \tag{9}$$

and $\Sigma^\pm$ is the self-energy, which is defined as

$$\Sigma^\pm = \langle V_{\text{imp}}G^\pm V_{\text{imp}}\rangle. \tag{10}$$

In the case under consideration, we can calculate the self-energy $\Sigma^\pm = \Sigma' \mp i\Gamma$ using an expression similar to that derived in Ref. [43]

$$\Sigma^\pm = \frac{n_i u_0^2}{(2\pi)^2}\int \frac{(\mu + rk^2 - \Sigma^\pm)\,kdk\,d\phi}{(\mu + rk^2 - \Sigma^\pm)^2 - \alpha_{Rk}^2k^2 - (\lambda k^3\cos 3\phi)^2}. \tag{11}$$

The function under integral in Eq. (11) decays as k^3 when $k \to \infty$. Thus, the value of this integral is determined by zeros of the denominator.

The value Γ is usually referred to as a disorder parameter or scattering rate. It determines the analytical properties of the Green's functions $G^\pm$, while Σ' is only a small correction to the chemical potential since we consider here only the case of small disorder. Thus, we can neglect the real part of the self-energy Σ' with the exception of some singular point, which will be specified below. If we put $\Sigma' = 0$ and have in mind that Γ is small in the limit of small disorder, we derive from Eq. (11) an explicit formula for the scattering rate

$$\Gamma(\mu) = \frac{n_i u_0^2}{(2\pi)^2}\int kdk\,d\phi\ \text{Im}G_0^+. \tag{12}$$

A. Bulk states

First, we consider the bulk states. In the simplest case, when λ and s tends to zero, we can derive an explicit formula for the scattering rate in two opposite limits, $r\Gamma/\alpha_R^2 \ll 1$ and

$r\Gamma/\alpha_R^2 \gg 1$. If the chemical potential μ is negative, we obtain from Eq. (12) following Ref. [44],

$$\Gamma(\mu < 0) = \Gamma_0 = \frac{n_i u_0^2}{4r}. \tag{13}$$

This value is independent of the chemical potential and the strength of the spin-orbit interaction. It is convenient to introduce dimensionless disorder parameter $\gamma_b = n_i u_0^2/(4\alpha_R^2)$. In these notations $\Gamma_0 = \alpha_R^2 \gamma_b / r$.

Effects of the spin-orbit coupling are not smeared by the disorder if $\alpha_R^2/r \gg \Gamma_0$ or, equivalently, $\gamma_b \ll 1$. We will call further the spin-orbit coupling strong if condition $\gamma_b \ll 1$ is satisfied. Otherwise, $\gamma_b \gg 1$, the spin-orbit coupling is weak.

In the helical regime, $\mu > 0$, the behavior of $\Gamma(\mu)$ depends on the system parameters. If the spin-orbit coupling is weak, $\gamma_b \gg 1$, we get that $\Gamma(\mu = 0) = \Gamma_0/2$ and $\Gamma(\mu)$ rapidly decays to zero with an increase of μ. In the opposite limit of strong strong spin-orbit coupling, $\gamma_b \ll 1$, we found from Eq. (12) that the scattering rate increases if $0 < \mu < \alpha_R^2/4r$:

$$\Gamma(\mu) = \frac{\Gamma_0 \alpha_R}{\sqrt{\alpha_R^2 - 4\mu r}}. \tag{14}$$

When the chemical potential attains the singularity point, $\mu = \alpha_R^2/4r$, the Fermi level crosses the bottom of the energy bands $E_\pm$ if s and $\lambda \to 0$ [see Eq. (2)]. If $\mu > \alpha_R^2/4r$, the Fermi level occurs in the energy gap. If we apply self-consistent Eq. (11) we get that at $\mu = \alpha_R^2/4r$ the real part of the self-energy vanishes and

$$\Gamma\left(\mu = \alpha_R^2/4r\right) = \Gamma_{\max} = \left(\frac{\alpha_R^2}{2r}\Gamma_0^2\right)^{1/3}. \tag{15}$$

Thus, in the helical regime the scattering rate increases significantly if the spin-orbit coupling is strong, $\Gamma_{\max}/\Gamma_0 = (1/2\gamma)^{1/3} \gg 1$.

In a more general case, the scattering rate $\Gamma(\mu)$ for the bulk states was calculated numerically using Eq. (11). The results are shown in Fig. 2 for the case of the strong spin-orbit coupling characteristic of the TIs. As we can see from the figure, the higher-order corrections to the spin-orbit coupling s and the hexagonal warping λ has a little impact on the value of the scattering rate in the case of the bulk states. In particular, a characteristic peak in $\Gamma(\mu)$ arises near the point $\mu = \alpha_R^2/4r$.

B. Surface states

For the surface states, we neglect a correction to the value of μ due to the real part of the self-energy in the limit of weak disorder, similar to the case of the bulk states. Thus, we can use Eq. (12) to calculate Γ.

In the simplest case r, λ, $s \to 0$ we obtain a well-known result [45,46],

$$\Gamma(\mu) = \gamma_b |\mu|. \tag{16}$$

When the chemical potential crosses the Dirac point, $\mu = 0$, we apply Eq. (11) and find that the real part of the self-energy vanishes while the imaginary part is exponentially small [45] $\Gamma(\mu = 0) = \alpha_R \min\{k_{\text{cut}}, \sqrt{\alpha_R/\lambda}, \sqrt{1/s}\} e^{-2/(\pi\gamma_b)}$, where k_{cut} is the momentum cutoff. That is, the scattering rate at the Dirac point is exponentially suppressed in the case of the strong spin-orbit coupling, $\gamma_b \ll 1$.

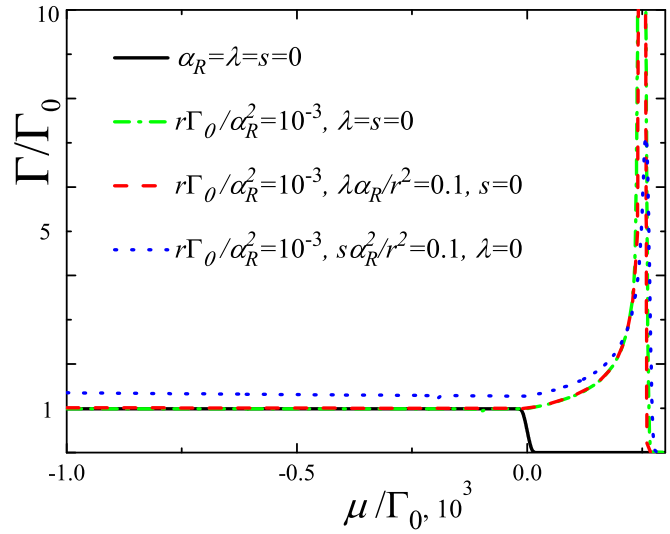

FIG. 2. Scattering rate Γ for the bulk states as a function of the dimensionless chemical potential μ/Γ_0. Black line corresponds to the case, when the spin-orbit interaction and the hexagonal warping are absent, $\alpha_R, \lambda \to 0$. Green line corresponds to $r\Gamma_0/\alpha_R^2 = 0.001$, $\lambda = 0$, and $s = 0$; red line to $r\Gamma_0/\alpha_R^2 = 0.001$, $\lambda\alpha_R/r^2 = 0.1$, and $s = 0$; blue line to $r\Gamma_0/\alpha_R^2 = 0.001$, $s\alpha_R^2/r^2 = 0.1$, and $\lambda = 0$.

In a more general case, the scattering rate for the surface states was calculated numerically with the help of Eq. (11). The dependence of $\Gamma(\mu)$ is shown in Fig. 3. We see that the scattering rate $\Gamma(\mu)$ is almost particle-hole symmetric since the spectrum of the surface states close to such a symmetry [see Fig. 1(e)].

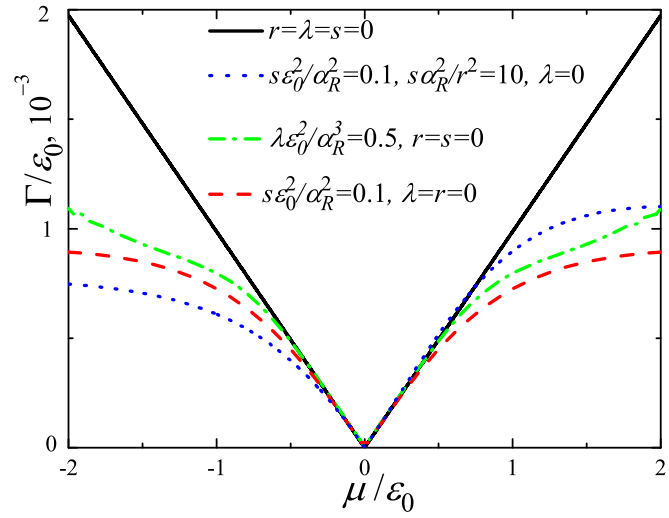

FIG. 3. Scattering rate Γ for the surface states as a function of the chemical potential μ for $\gamma_b = 0.001$. Black line corresponds to the case $r = s = \lambda = 0$, green line to $\lambda\varepsilon_0^2/\alpha_R^3 = 0.5$, $s = r = 0$, red line to $s\varepsilon_0^2/\alpha_R^2 = 0.1$, $\lambda = r = 0$, blue line to $s\varepsilon_0^2/\alpha_R^2 = 0.1$, $\lambda = 0$. Normalization parameter is chosen as $\varepsilon_0 = \alpha_R k_{\text{cut}}/10$ where k_{cut} is the cutoff momentum.

The self-energy is proportional to the identity matrix. This allows to obtain an explicit expression for the impurity averaged Green's function. We can rewrite Eq. (8) as $G^{\pm} = (1 + \Sigma G_0^{\pm})^{-1} G_0^{\pm}$ or

$$G^{\pm} = \frac{\mu + rk^2 \pm i\Gamma - \alpha_{Rk}(k_x\sigma_y - k_y\sigma_x) - \lambda k^3 \cos 3\phi\, \sigma_z}{(\mu + rk^2 \pm i\Gamma)^2 - \alpha_{Rk}^2 k^2 - \lambda^2 k^6 \cos^2 3\phi}. \tag{17}$$

Therefore, the expression for $G^{\pm}$ is given by an equation similar to Eq. (9) for $G_0^{\pm}$, in which $\pm i0$ is replaced by $\pm i\Gamma$. We characterize disorder by a single value Γ neglecting renormalization of the chemical potential.

IV. VERTEX CORRECTIONS

In the SCBA, following the approach described in Ref. [43], we can derive an equation for the vertex corrected velocity operator [46]

$$V_\alpha(\mathbf{k}) = v_\alpha(\mathbf{k}) + \frac{n_i u_0^2}{(2\pi)^2} \int G^+(\mathbf{k}) V_\alpha(\mathbf{k}) G^-(\mathbf{k}) d^2\mathbf{k}. \tag{18}$$

We present here the derivation of V_x; results for V_y can be obtained just by the substitution $x(y) \to y(x)$.

It is easy to show that $n_i u_0^2 \int G^+ v_x G^- d^2\mathbf{k}/(2\pi)^2 = \zeta\sigma_y$ and $n_i u_0^2 \int G^+ \sigma_y G^- d^2\mathbf{k}/(2\pi)^2 = \kappa\sigma_y$, where ζ and κ are scalars. In these notations we obtain from Eq. (18) that

$$V_x = v_x + (\alpha_R^{VC} - \alpha_R)\sigma_y, \quad \alpha_R^{VC} = \alpha_R + \frac{\zeta}{1-\kappa}. \tag{19}$$

We begin our consideration with the bulk states and derive some analytical results in the simplest case, when s and λ are zero. Under such conditions and if $\mu < 0$, the vertex corrected Rashba coupling is small, $\alpha_R^{VC} \ll \alpha_R$, either at weak, $\gamma_b \gg 1$, or strong, $\gamma_b \ll 1$, Rashba coupling in accordance with the results of previous works (see, e.g., Refs. [12,13]). However, in the case of strong Rashba coupling, when the chemical potential is positive and lies in the interval $0 < \mu < \alpha_R^2/4r$, the vertex corrected α_R^{VC} is comparable to its bare value α_R

$$\frac{\alpha_R^{VC}}{\alpha_R} = \frac{\alpha_R - \sqrt{\alpha_R^2 - 4r\mu}}{\alpha_R + \sqrt{\alpha_R^2 - 4r\mu}}. \tag{20}$$

Numerically calculated dependence of the vertex correction to the Rashba coupling for the bulk states on the chemical potential, $\alpha_R^{VC}(\mu)$, is shown in Fig. 4 for a more general situation. As we can see, the higher-order corrections to the spin-orbit coupling and the hexagonal warping significantly enhances α_R^{VC} in the region $\mu < 0$. Nevertheless, its value is still much smaller than the bare value α_R. When $\mu < 0$ (in the helical regime), $\alpha_R^{VC}(\mu)$ is of the order of α_R and almost independent of s and λ.

For the surface states, in the case r, s, $\lambda = 0$ and $\gamma_b \ll 1$, we get that away from the Dirac point, $\mu \gg \Gamma$, the vertex correction is $\alpha_R^{VC} = 2\alpha_R$, while α_R^{VC} vanishes at $\mu = 0$, as it have been obtained in Refs. [46,47]. Numerically calculated dependence of the vertex correction α_R^{VC} on the chemical potential is shown in Fig. 5 for the parameters characteristic of the surface states. The presence of the hexagonal warping slightly increases α_R^{VC}, while the existence of the finite mass term r leads to the particle-hole asymmetry. Taking into account correction to the spin-orbit coupling s results in a increase of α_R^{VC} if the chemical potential is away from the Dirac point.

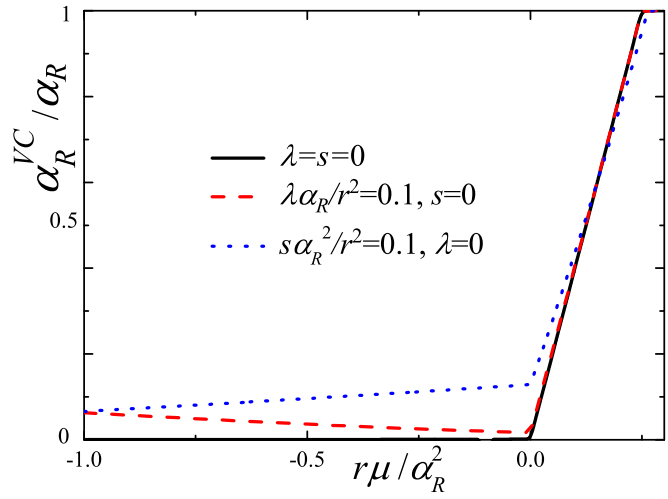

FIG. 4. Dependence of α_R^{VC} for the bulk states on the chemical potential, $\gamma_b = 0.001$. Black line corresponds to $\lambda = s = 0$, red line to $\lambda\alpha_R/r^2 = 0.1$ and $s = 0$, blue line to $s\alpha_R/r^2 = 0.1$ and $\lambda = 0$.

V. SPIN CONDUCTIVITY FROM THE STATES AT THE FERMI SURFACE

Now we use the results obtained in the previous sections and Eqs. (5) and (6) to calculate the contribution to the spin conductivity due to the states at the Fermi surface. In this way, we obtained that in the considered approach the term $\sigma_{\alpha\beta}^{Iy}$ vanishes exactly. Thus, we should to compute only the term $\sigma_{\alpha\beta}^{I\gamma}$.

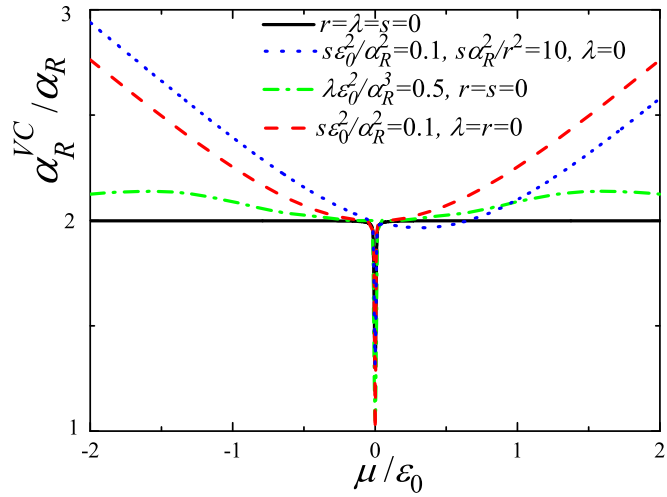

FIG. 5. Dependence of the vertex correction α_R^{VC} on the chemical potential for the surface states, $\gamma_b = 0.001$. Black line corresponds to the case $r = \lambda = s = 0$, blue line to $s\varepsilon_0^2/\alpha_R^2 = 0.1$, $s\alpha_R^2/r^2 = 10$, and $\lambda = 0$, green line to $\lambda\varepsilon_0^2/\alpha_R^3 = 0.5$ and $r = s = 0$, red line to $s\varepsilon_0^2/\alpha_R^2 = 0.1$ and $r = \lambda = 0$.

The isotropic tensor component $\sigma_{xy}^{Iz} = -\sigma_{yx}^{Iz}$ is the only term that persists in the system in the case of zero hexagonal warping. All other components are anisotropic and they are non-zero only if $\lambda \neq 0$. The measured value of the spin conductivity depends on the mutual orientation of the current and the crystal axes. So, it is convenient to relate the spin conductivity tensor components in the crystal axes (x, y) with that related to the current direction, $(\bar{x}, \bar{y})$. New coordinates are obtained by anticlockwise rotation by the angle θ along the crystal axes. We assume that the current is directed along $\bar{x}$-axis. In this coordinates we have

$$\begin{aligned}
&\sigma_{\bar{x}\bar{x}}^{I\bar{x}} = -\sigma_{\bar{y}\bar{y}}^{I\bar{y}} = -\sigma_{\bar{y}\bar{y}}^{I\bar{x}} = -\sigma_{\bar{y}\bar{x}}^{I\bar{y}} = \sigma_{xx}^{Ix}\cos 3\theta,\\
&\sigma_{\bar{x}\bar{y}}^{I\bar{x}} = \sigma_{\bar{x}\bar{x}}^{I\bar{y}} = \sigma_{\bar{y}\bar{x}}^{I\bar{x}} = -\sigma_{\bar{y}\bar{y}}^{I\bar{y}} = -\sigma_{xx}^{Ix}\sin 3\theta,\\
&\sigma_{\bar{x}\bar{x}}^{Iz} = \sigma_{\bar{y}\bar{y}}^{Iz} = 0.
\end{aligned} \tag{21}$$

Therefore, it is sufficient to calculate σ_{xy}^{Iz} and σ_{xx}^{Ix}.

We derive from Eq. (5)

$$\begin{aligned}
\sigma_{xy}^{Iz} &= \sigma_0^z \int k\,dk\,d\phi\ \frac{2r\Gamma\alpha_{Rk}k^2\left(\alpha_R^{VC} + \alpha_R s k^2\right)}{\pi^2 E_g(k,\phi)}\\
\sigma_{xx}^{Ix} &= \sigma_0^z \int k\,dk\,d\phi\ \frac{r\alpha_R\Gamma\lambda k^4(3+2sk^2)}{\pi^2 E_g(k,\phi)}\\
E_g &= 4\Gamma^2(\mu + rk^2)^2 + (\Gamma^2 - E_- E_+)^2,
\end{aligned} \tag{22}$$

where $\sigma_0^z = e/(8\pi)$ is the spin conductivity quanta and $E_\pm$ is given by Eq. (2). As we can see, the isotropic spin conductivity component σ_{xy}^{Iz} is proportional to α_R^{VC} if we neglect the higher-order correction to the spin-orbit coupling. This value increases significantly in the helical state $\mu > 0$. The anisotropic component σ_{xx}^{Ix} is proportional to the hexagonal warping strength λ, the vertex corrections does not affect it.

First, we calculate the contribution to the spin conductivity from the bulk states. The results are shown in Fig. 6. As we can see from the top panel in Fig. 6, the isotropic spin conductivity component σ_{xy}^{Iz} is suppressed when the chemical potential is negative. It occurs since the vertex correction α_R^{VC} is small in this region of μ. However, when $0 < \mu < \alpha_R^2/4r$, the value of α_R^{VC} is comparable to α_R and the value of σ_{xy}^{Iz} increases significantly. Note that s and λ produces a weak effect on σ_{xy}^{Iz} in this range of μ. If $\mu > \alpha_R^2/(4r)$, the spin conductivity vanishes since the density of states on the Fermi disappears.

The results for the anisotropic component of the spin conductivity σ_{xx}^{Ix} are presented in the bottom panel of Fig. 6. This value decreases almost linearly with an increase of the chemical potential if $\mu < 0$ and, when $\mu > 0$, it has a small peak near $\mu = \alpha_R^2/4r$. The value σ_{xx}^{Ix} also demonstrate almost a linear growth with an increase of the coefficients λ and s.

The dependencies of the isotropic and anisotropic components of the spin conductivity on μ for the surface states are shown in Fig. 7. Both these values have minima at the Dirac point $\mu = 0$ and particle-hole asymmetry that is smaller for larger s. Note that σ_{xy}^{Ix} and σ_{xx}^{Ix} for the surface states decreases with an increase of the next-order correction to the spin-orbit coupling coefficient s.

The effect of disorder on the spin conductivity $\sigma_{\alpha\beta}^{I\gamma}$ is illustrated in Fig. 8. Both surface and bulk conductivities are

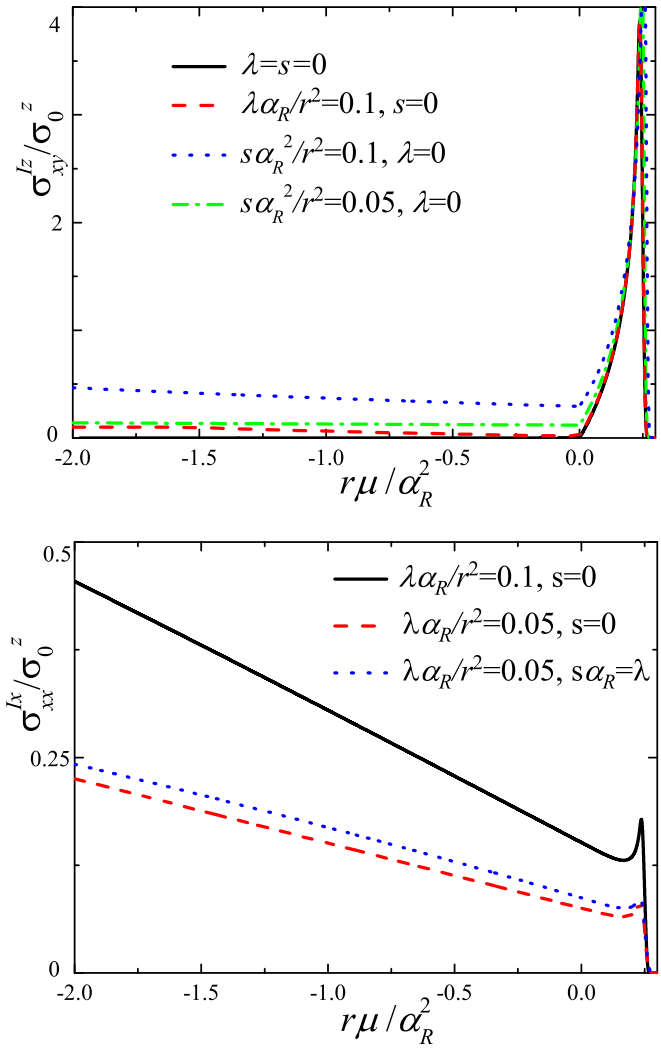

FIG. 6. Isotropic spin conductivity σ_{xy}^{Iz} (top) and anisotropic spin conductivity σ_{xx}^{Ix} (bottom) for the bulk states as a function of the chemical potential μ, $\gamma_b = 0.01$. In the top panel black line corresponds to $s = \lambda = 0$, red line to $\lambda\alpha_R/r^2 = 0.1$ and $s = 0$, blue line to $s\alpha_R^2/r^2 = 0.1$ and $\lambda = 0$, green line to $s\alpha_R^2/r^2 = 0.05$ and $\lambda = 0$. In the bottom panel black line corresponds to $\lambda\alpha_R/r^2 = 0.1$ and $s = 0$, red to $\lambda\alpha_R/r^2 = 0.05$ and $s = 0$, blue line to $\lambda\alpha_R/r^2 = 0.05$ and $s = \lambda/\alpha_R$.

robust against disorder in the weak scattering limit, $\gamma_b \ll 1$. Moreover, the topologically protected surface terms are robust even in the case of higher disorder, $\gamma_b \sim 1$, while the components of the bulk conductivity decrease significantly in this limit. However, the SCBA is not correct for a strong disorder $\gamma_b \sim 1$ and more advanced techniques are required to study the robustness of the spin conductivity of the surface states in such regime.

VI. SPIN CONDUCTIVITY FROM THE FILLED STATES

Here we calculate the contribution to the spin conductivity from the filled states using Eq. (7) and the obtained above results for the disorder parameter Γ. Note that the vertex corrections do not affect this part of the spin conductivity. Similar to the spin conductivity from the states at the Fermi

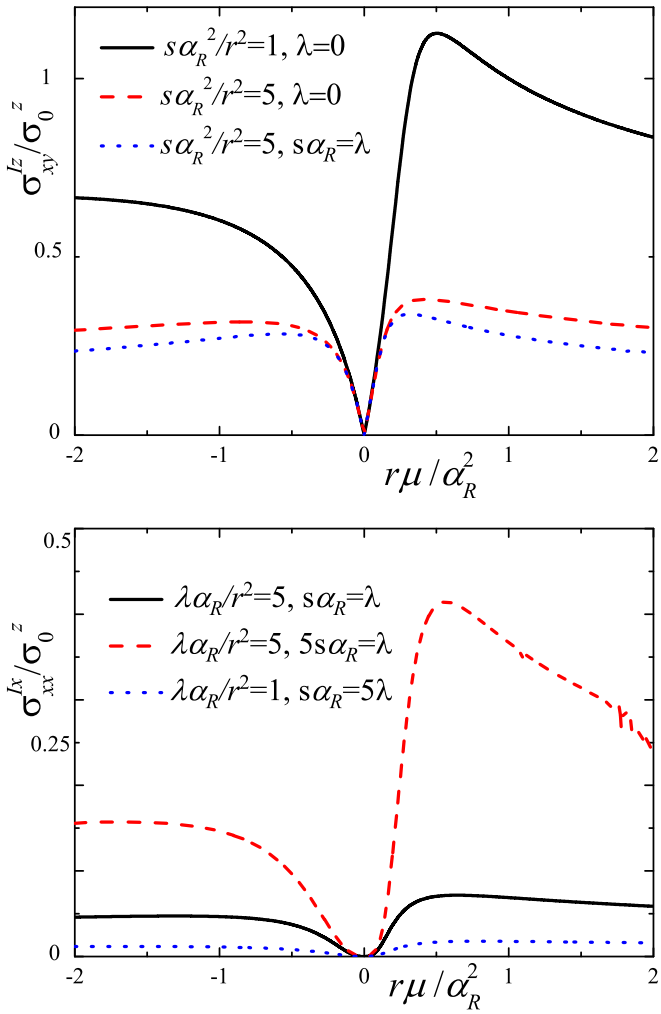

FIG. 7. Isotropic spin conductivity σ_{xy}^{Iz} (top) and anisotropic spin conductivity σ_{xx}^{Ix} (bottom) for the surface states as a function of the chemical potential, $\gamma_b = 0.01$. In the top panel black line corresponds to $s\alpha_R^2/r^2 = 1$ and $\lambda = 0$, red line to $s\alpha_R^2/r^2 = 5$ and $\lambda = 0$, blue line to $s\alpha_R^2/r^2 = 5$ and $\lambda = s\alpha_R$. In the bottom panel black line corresponds to $s\alpha_R^2/r^2 = 5$ and $\lambda = s\alpha_R$, red line to $s\alpha_R^2/r^2 = 1$ and $\lambda = 5s\alpha_R$, blue line to $s\alpha_R^2/r^2 = 5$ and $\lambda = s\alpha_R/5$.

surface, the spin conductivity from the filled states has an isotropic component σ_{xy}^{IIIz} and anisotropic one σ_{xx}^{IIIx}. The isotropic component, $\sigma_{xy}^{IIIz} = -\sigma_{yx}^{IIIz}$, is the only term that persists in the system in the absence of the hexagonal warping. The anisotropic components are nonzero only if $\lambda \neq 0$. In the rotated coordinates $(\bar{x}, \bar{y})$, the components of tensor $\sigma_{\alpha\beta}^{III\gamma}$ transform similar to $\sigma_{\alpha\beta}^{I\gamma}$, see Eq. (21).

We obtain by means of Eq. (7)

$$\sigma_{xy}^{IIIz} = \sigma_0^z \int [\Theta(E_1) - \Theta(E_2)] k\, dk\, d\phi \frac{2rk\alpha_{Rk}^2}{\pi E_s}$$

$$\sigma_{xx}^{IIIx} = \sigma_0^z \int [\Theta(E_1) - \Theta(E_2)] k\, dk\, d\phi \frac{rk^4\alpha_R\lambda(3+2k^2 s)}{\pi E_s}$$

$$E_s = \sqrt{\alpha_{Rk}^2 + \lambda^2 k^6 \cos^2 3\phi}\left[4\alpha_{Rk}^2 k^2 + \lambda^2 k^6 \cos^2 3\phi + \Gamma^2\right], \quad (23)$$

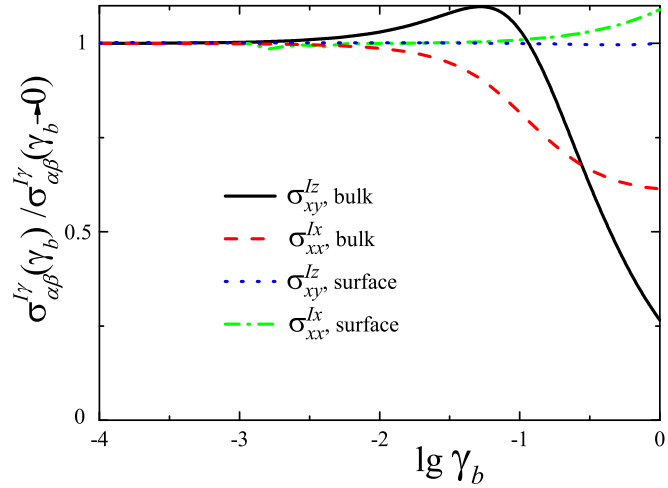

FIG. 8. Contribution to the spin conductivity from the states at the Fermi level, $\sigma_{\alpha\beta}^{I\gamma}$, for the bulk and surface states as a function of disorder strength γ_b. For all curves $\mu = -\alpha_R^2/r$. Black line corresponds to the contribution from the bulk states in σ_{xy}^{Iz} for s, and $\lambda = 0$, red line to the contribution from the bulk states in σ_{xx}^{Ix} for $\lambda\alpha_R/r^2 = 0.1$ and $s = 0$, blue line is the contribution from the surface states in σ_{xy}^{Iz} for $s\alpha_R^2/r^2 = 5$ and $\lambda = 0$, green line is the contribution from the surface states in σ_{xx}^{Ix} for $s\alpha_R^2/r^2 = 5$ and $\lambda = s\alpha_R$.

where $\Theta(x)$ is the Heaviside step function.

We start with the bulk spin conductivity. In the clean limit, $\Gamma = 0$, and zero third-order corrections, $\lambda = 0$ and $s = 0$, we get that $\sigma_{xy}^{IIIz} = \sigma_0^z\sqrt{1 - 4\mu r/\alpha_R^2}$ if $\mu > 0$ and $\sigma_{xy}^{IIIz} = \sigma_0^z$ if $\mu < 0$. The latter relation is a well-known result for a spin Hall conductivity [10,42]. In a more general case, the results were obtained numerically and presented in Fig. 9. As we can see from top panel of this figure, the hexagonal warping has a little effect on the value of the isotropic spin conductivity, while the correction to the spin-orbit coupling s enhances it. According to bottom panel of Fig. 9, the anisotropic part of the spin conductivity, σ_{xx}^{IIIx}, decays monotonically with the increase of the chemical potential. It increases almost linearly with the increase of the hexagonal warping strength λ. The bulk spin conductivity becomes zero when the chemical potential crosses the bottom of the conduction band and occurs in the energy gap.

The results for the contribution to the spin conductivity from the surface states are shown in Fig. 10. We see that both $\sigma_{xy}^{IIIz}(\mu)$ and $\sigma_{xx}^{IIIz}(\mu)$ have maxima at the Dirac point $\mu = 0$ and decreases with the increase of $|\mu|$ (in contrast to the contribution from the states at the Fermi level, Fig. 7). These functions are more or less particle-hole symmetric. From Fig. 10, we see that the value of isotropic spin conductivity σ_{xy}^{IIIz} decreases with the increase of the higher-order momentum corrections λ and s. The value of anisotropic spin conductivity σ_{xx}^{IIIx} increases with the increase of hexagonal warping strength λ and decreases with the increase of s.

The dependence of $\sigma_{\alpha\beta}^{III\gamma}$ on the disorder parameter Γ is shown in Fig. 11. We obtain that the spin conductivity from the filled states is robust against disorder if $\gamma_b \ll 1$. If

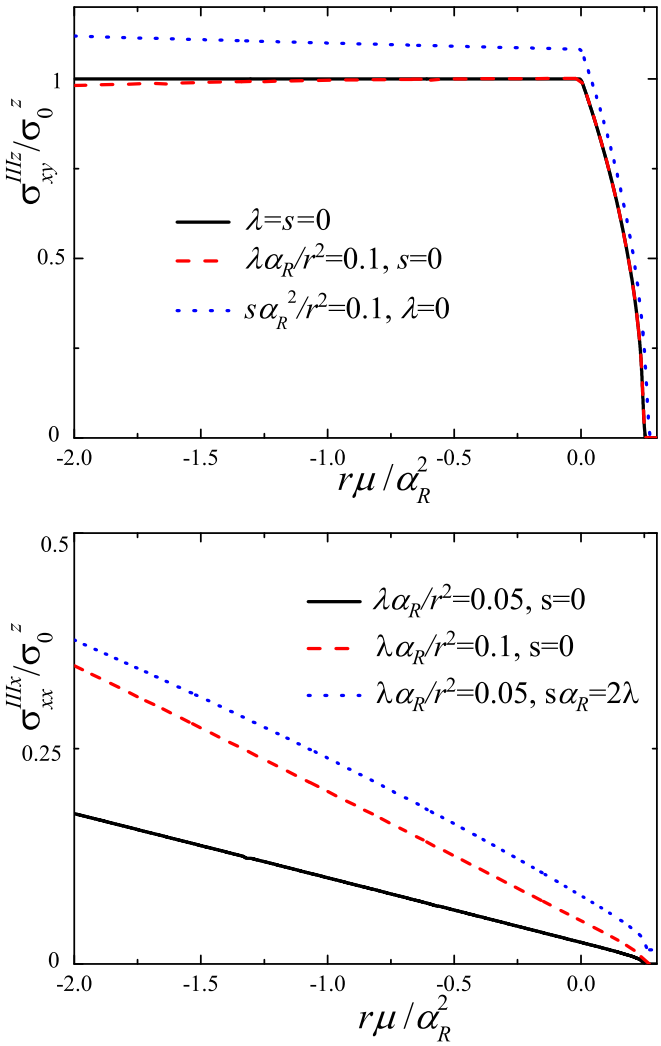

FIG. 9. Isotropic spin conductivity σ_{xy}^{IIIz} (top) and anisotropic spin conductivity σ_{xx}^{IIIx} (bottom) for the bulk states as a function of the chemical potential in the clean limit, $\Gamma = 0$. In the top panel black line corresponds to λ and $s = 0$, red line to $\lambda\alpha_R/r^2 = 0.1$ and $s = 0$, blue line to $s\alpha_R^2/r^2 = 0.1$ and $\lambda = 0$. In the bottom panel black line corresponds to $\lambda\alpha_R/r^2 = 0.05$ and $s = 0$, red line to $\lambda\alpha_R/r^2 = 0.1$ and $s = 0$, blue line to $\lambda\alpha_R/r^2 = 0.1$, $s\alpha_R = 2\lambda$.

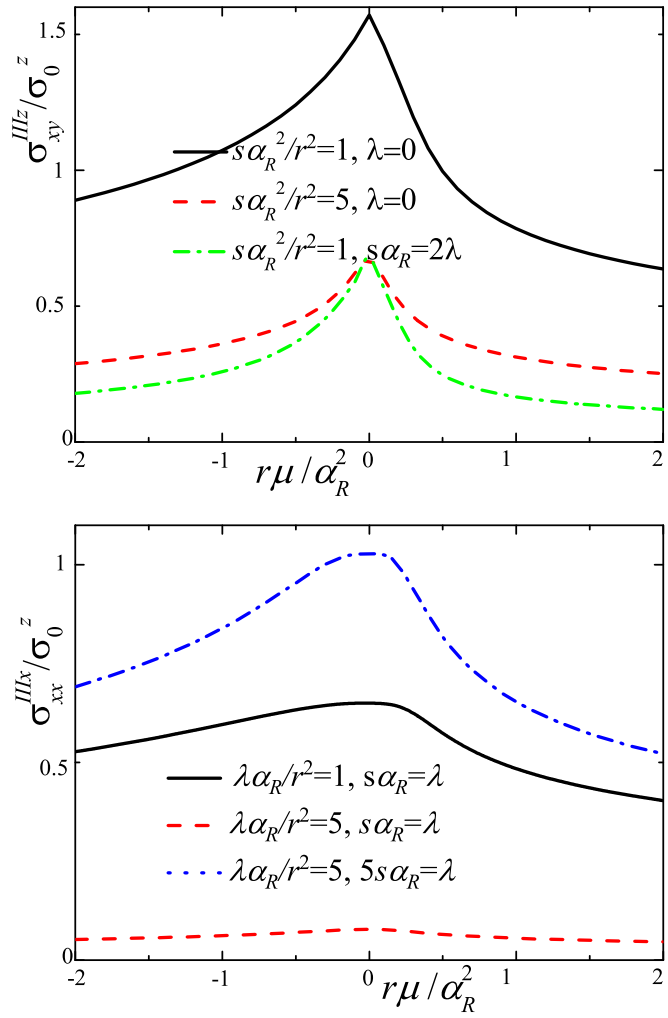

FIG. 10. Isotropic spin conductivity σ_{xy}^{IIIz} (top) and anisotropic spin conductivity σ_{xx}^{IIIx} (bottom) for the surface states as a function of the chemical potential for $\Gamma = 0$. Black line corresponds to $s\alpha_R^2/r^2 = 5$ and $\lambda = 0$, red line to $s\alpha_R^2/r^2 = 1$ and $\lambda = 0$, green line to $s\alpha_R^2/r^2 = 1$ and $2\lambda = s\alpha_R$.

the disorder is stronger, $\gamma_b \sim 1$, both the bulk and surface conductivities are suppressed.

VII. EVALUATION OF CHARACTERISTIC PARAMETERS

In this section, we demonstrate that the values of the parameters used above for the calculation of the spin conductivity are reasonable. We can extract information on the disorder strength from Ref. [48]. The imaginary part of the self-energy for the surface states in Bi_2Te_3 can be estimated from the ARPES data presented in Ref. [48] as a half-width of the quasiparticle peak: $\Gamma \approx 1$ meV and peak position corresponds to $\mu \approx 100$ meV. Thus, we get $\gamma_b \approx 10^{-2}$. This is an upper limit for the disorder strength, since, for example, electron-phonon and electron-electron interactions also contribute to the blurring of the quasiparticle peak. The alternative indirect estimate we obtain as follows. The STM data from Ref. [49] shows that for a clean surface of Bi_2Te_3 there exists one defect approximately per Å^2. We suppose that a typical impurity potential is of the order of the chemical potential μ (which was about 200 meV). This assumption is true, e.g., for vacations. The Fermi velocity for the surface states was evaluated in Ref. [50] as $\alpha_R \approx 3$ eV Å^{-1}. Then, we get $\gamma_b \approx 10^{-3}$–10^{-2}. However, the value of the Fermi velocity for the surface states differs from sample to sample: lower Fermi velocities down to $\alpha_R \approx 0.03$ eV Å^{-1} have been reported [51]. The value of the Rashba coupling for the bulk states is proportional to the spin splitting of the bands. This value can be tuned by doping from 0 up to $\alpha_R \approx 1.3$ eV Å^{-1} for Bi_2Se_3, for BiTeI this value is even larger $\alpha_R \approx 3.1$ eV Å^{-1} [52]. Thus, the value of α_R for the bulk states with large spin splitting can have the same order as for the surface states. Also, the electron mass for the bulk states [53] is close to that for the surface states [54]. Thus it is reasonable to expect that γ_b for the bulk states with large

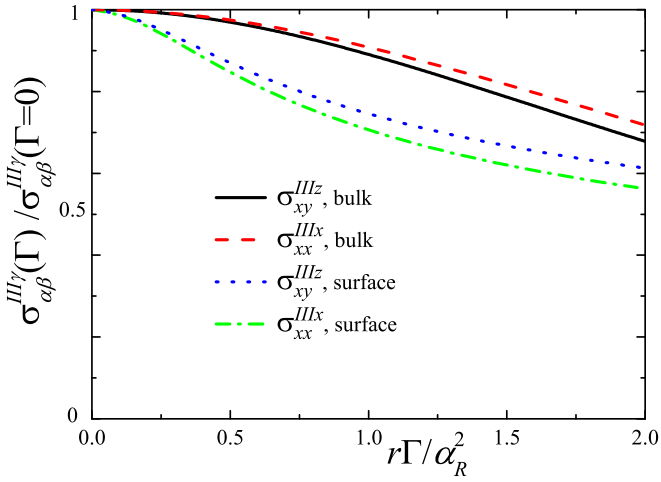

FIG. 11. Bulk and surface contributions to the spin conductivity from the filled states, $\sigma^{IIIγ}_{αβ}$, as a function of disorder parameter Γ at $\mu = -\alpha_R^2/r$. Black line corresponds to the isotropic component due the bulk states, σ^{IIIz}_{xy}, for s and $\lambda = 0$, red line presents the anisotropic component due to the bulk states, σ^{IIIx}_{xx}, for $\lambda\alpha_R/r^2 = 0.1$ and $s = 0$, blue line is the isotropic component due to the surface states, σ^{IIIz}_{xy}, for $s\alpha_R^2/r^2 = 5$ and $\lambda = 0$, green line is the anisotropic component due to the surface states, σ^{IIIx}_{xx}, for $s\alpha_R^2/r^2 = 5$ and $\lambda = s\alpha_R$.

Rashba splitting would of the same order as for the surface states.

In Table I we put estimated values of the dimensionless parameters for Bi_2Se_3. These values were obtained by fitting the ARPES data presented in Refs. [54] and [55]. Here subscripts b and s stand for the bulk and surface states, respectively. In general, the positions of the Dirac cone for the surface states is different from the position of zero μ for the bulk states (as it was defined in Fig. 1). Thus, $\mu_s \neq \mu_b$. Naturally, we can extract reliable values of parameters α_R, r, λ, and s only for the surface states. We assume that the characteristics α_R, r, and λ are the same for the surface states and bulk states, while $s_b = 0.1 s_s$. We believe that such a choice does not affect the results within an order of magnitude.

We calculate the components of the spin conductivity for the set of parameters from Table I and for the dimensionless disorder strength $\gamma_b = 10^{-3}$ estimated above. The results are presented in Table II. We see that typically the isotropic, σ^z_{xy}, and anisotropic, σ^x_{xx}, components of the spin conductivity has the same order of magnitude. The contribution from the states at the Fermi level is comparable to the contribution from the filled states. The spin conductivity of the surface states is of the same order as the conductivity from the bulk states per layer for large values of the spin splitting. However, if Rashba spin splitting of the bulk states is small $\gamma_b \sim 1$ then spin

TABLE I. Dimensionless parameters extracted from the experimental data of Refs. [54] and [55].

	$\lambda\alpha_R/r^2$	$r\mu_b/\alpha_R^2$	$r\mu_s/\alpha_R^2$	$s_b\alpha_R^2/r^2$	$s_s\alpha_R^2/r^2$
Bi_2Se_3	0.1	0.1	−0.5	0.07	0.7

TABLE II. Components of the spin conductivity calculated using the parameters from Table I and $\gamma_b = 10^{-3}$.

	$\sigma^{Iz}_{xy}/\sigma^z_0$	$\sigma^{Ix}_{xx}/\sigma^z_0$	$\sigma^{IIIz}_{xy}/\sigma^z_0$	$\sigma^{IIIx}_{xx}/\sigma^z_0$
Bulk states per layer	1.67	1.47	0.5	0.22
Surface states	0.57	0.07	0.8	1.02

conductivity for the bulk states is suppressed in comparison with spin conductivity of the surface states.

Using the estimated above values of parameters, we calculate the dependence of the total spin conductivity, $\sigma^{\gamma}_{\alpha\beta} = \sigma^{I\gamma}_{\alpha\beta} + \sigma^{III\gamma}_{\alpha\beta}$, on the chemical potential. The results for the bulk and surface states are shown in Fig. 12. As we can see from the top panel in Fig. 12, the isotropic bulk spin conductivity slowly decreases from the plateau with an increase of μ, then, has a peak, and finally drops to zero. It is rather high in the helical state. As for the anisotropic component, σ^x_{xx}, its value is considerably smaller than σ^z_{xy}. It monotonously decreases to zero with the growth of the chemical potential. The

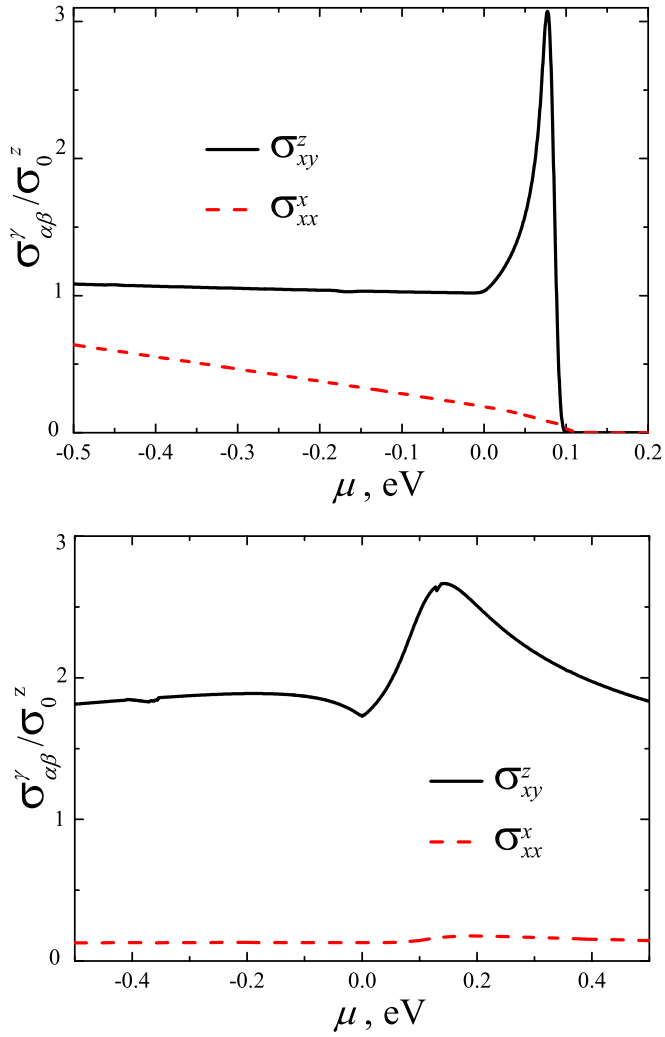

FIG. 12. Total bulk spin conductivity per layer (top) and total surface spin conductivity (bottom) calculated for parameters from Table I and $\gamma_b = 10^{-3}$. Black line shows isotropic spin conductivity σ^z_{xy} and red line shows anisotropic component σ^x_{xx}.

spin conductivity due to the surface states does not depend crucially on the chemical potential, Fig. 12. The anisotropic component of the surface spin conductivity is much smaller than the isotropic one.

VIII. DISCUSSION

The spin conductivity quanta can be expressed in the dimensional units as $\sigma_0^z \approx (\hbar/2e)\,2\cdot 10^{-5}\,\Omega^{-1}$. In the previous section we estimate that the spin conductivity per conducting layer (either bulk or surface) is of the order of σ_0^z. The distance between the layers in the TIs l is of the order of 1 nm. Then, the specific (volume) spin conductivity can be estimated as $\sigma_{xy}^z/l \sim \sigma_{xx}^x/l \sim (\hbar/2e)\,2\cdot 10^4\,\Omega^{-1}\mathrm{m}^{-1}$. These values are close to that directly measured in Bi_2Se_3 [20].

It has been speculated that the surface states can generate large spin currents observed in the experiment [23–25]. According to our study, the surface states cannot produce very large spin current and the spin conductivity of the surface states typically has the same value as the spin conductivity of the bulk states per layer if spin splitting of the bulk bands is large. So, our work confirms the experiments that show that spin conductivity mainly arises from the bulk states for a multilayer TI [20,26]. In this case increasing the number of layers has no effect on the value of spin conductivity, as it has been observed recently [56]. Also, it can explain the experiment, where the spin conductivity is small when the bulk of the TI sample is insulating, and the spin conductivity increases, when the bulk is conducting [22]. If spin splitting of the bulk bands is small $\gamma_b \ll 1$ then bulk spin conductivity is suppressed in comparison with the surface spin conductivity. In this case spin conductivity is mainly carried by the surface states $\sigma_{xy}^z/L \sim 2\sigma_{xy}^z(\mathrm{surf})/L$, where L is the film thickness, and decreases with increase of thickness of film as it was observed in some experiments [17].

In the present study we can not explain a colossal spin conductivity in BiSb [56] and $(Bi_{0.5}Sb_{0.5})_2Te_3$ [18], which is about two orders of magnitude higher than our estimation. This discrepancy may occur for the following reasons. Our model consists only of two bands and cannot capture complex multiband effects. For BiSb it is shown that the gap between conduction and valence band is small or absent [34]. This means that many bands contribute to the spin conductivity and there might be some interaction between those bands that our model cannot capture. Yet large spin splitting of the bulk bands [57] can serve as a confirmation of our prediction that large Rashba coupling leads to the high spin conductivity. Also, in our consideration we do not take into account the effects of a magnetic field. The external magnetization (which is typically presented in the experiments [18]) could enhance or reduce the spin conductivity. However, we believe that it is not the key factor if the magnetic field is not too large. It have been argued in Ref. [20] that different values of the spin conductivity can be a result of different fitting procedures of the experimental data. In Ref. [18] spin conductivity is measured indirectly.

We want to emphasize that the parameter α_R is the Rashba coupling for the bulk states. Under certain conditions this Rashba coupling can be quite large [58]. Experimentally, Rashba coupling α_R for the bulk states can be tuned by the doping [59] or strain [60].

In Refs. [12,13] it has been shown that the vertex corrections lead to suppression of the Rashba coupling and, consequently, the (bulk in the TIs) spin conductivity from the states at the Fermi level is damped. However, in these papers the helical state, $0 < \mu < \alpha_R^2/4r$, has not been considered. According to our analysis, in such phase, the vertex-corrected Rashba spin-orbit coupling is comparable to its bare value α_R. So, a quite significant contribution to the spin current can be observed even from the bulk states. The vertex corrections also increases the contribution from the surface states to the spin conductivity.

The bulk spin conductivity is robust against disorder if the spin splitting is large in comparison with a disorder, $\gamma_b \ll 1$. Otherwise, these contributions to the spin conductivity are suppressed, see Figs. 8 and 11. The surface spin conductivity is robust against disorder even if a disorder is not weak, $\gamma_b \sim 1$. The nature of robustness of the surface spin conductivity is similar to the robustness of the surface charge conductivity against disorder and arises due to suppression of the backscattering. However, the study of the spin conductivity of the surface states in case of strong disorder deserves future studies.

We neglect the effect of the finite hybridization between the different sides of the thin film. In principle, this hybridization can open a gap in the spectrum of the surface states. However, if there is at least six layers then the gap due to hybridization of the different sides vanishes [61] and we can consider each side of the film independently. Effects of the finite thickness on the spin conductivity are studied in the paper that we are preparing for publication [62].

The surface spin conductivity in a thin layer of TI with a cubic lattice have been studied in Ref. [35] without taking into account the vertex corrections. The authors of the latter paper argue that the dependence of the surface spin conductivity on the disorder and chemical potential is weak. Our analysis confirms these results qualitatively, see Figs. 8, 11, and 12. However, vertex corrections increase spin conductivity of the states at the Fermi energy approximately by factor of 2, so this agreement between results is qualitative not quantitative.

The bulk spin conductivity can be tuned by a changing the chemical potential. Adjusting the chemical potential to the vicinity of the bottom of electron band, $\mu = \alpha_R^2/4r$, we can attain the largest spin currents, see Fig. 12. The tuning of the spin conductivity contribution from the filled states by changing the chemical potential has been demonstrated numerically in Ref. [34]. The dependence of the spin Hall angle on the chemical potential has been measured in the experiments [19]. However, the observed result can be explained not only by the present analysis but also by the particle-hole asymmetry of the charge current.

In the experiment, the components of the spin conductivity tensor are measure in the coordinate axes $\bar{x}$, $\bar{y}$ related to the current. In Ref. [21] the spin conductivity component $\sigma_{\bar{x}\bar{x}}^{y}$ was measured in $BiSbTeSe_2$. The authors observed different sign of this value in different samples. According to the conductivity tensor transformation presented in Sec. V, Eq. (21), the measured conductivity should be anisotropic and depends on the angle θ between the current and crystallographic x axis

as $\sigma^{y}_{x\bar{x}} = -\sigma^{x}_{xx} \sin 3\theta$. Thus, different sign of the measured spin conductivity may be due to the different orientation of the current leads with respect to the crystallographic axes in different samples.

We used Kubo formalism to study spin conductivity to incorporate vertex corrections and contributions from the filled states and from the states at the Fermy energy. Also, similar calculations can be done using kinetic approach that may be computationally beneficial for a complex systems [63]. This approach can be used to study spin-orbit torques in different systems as well [64].

In conclusion, we found that hexagonal warping gives rise to the additional anisotropic components in the spin conductivity. For the bulk states spin conductivity is enhanced at the helical regime where only one spin-split band occurs at the Fermi energy due to large vertex corrected spin orbit coupling. Spin conductivity of the bulk states in robust against disorder if spin splitting of the bands larger than disorder broadening; otherwise, spin conductivity is suppressed. Spin conductivity of the surface states is robust against disorder and have the similar value to the conductivity of the bulk states with large Rashba coupling per layer.

ACKNOWLEDGMENTS

The work was partially performed in P. N. Lebedev Physical Institute of the RAS under support of Russian Science Foundation Grant (No. 17-12-01544). R.S.A.'s work was supported by the Foundation for the Advancement of Theoretical Physics and Mathematics "BASIS", RFBR according to the research project 19-32-80014, ICFPM (MMK) of Education and Science of the Russian Federation, Grant No. 14Y26.31.0007.

[1] M. Z. Hasan and C. L. Kane, Colloquium: Topological insulators, Rev. Mod. Phys. **82**, 3045 (2010).

[2] L. Fu, Hexagonal Warping Effects in the Surface States of the Topological Insulator Bi_2Te_3, Phys. Rev. Lett. **103**, 266801 (2009).

[3] K. Kuroda, M. Arita, K. Miyamoto, M. Ye, J. Jiang, A. Kimura, E. E. Krasovskii, E. V. Chulkov, H. Iwasawa, T. Okuda *et al.*, Hexagonally Deformed Fermi Surface of the 3D Topological Insulator Bi_2Se_3, Phys. Rev. Lett. **105**, 076802 (2010).

[4] C. M. Wang and F. J. Yu, Effects of hexagonal warping on surface transport in topological insulators, Phys. Rev. B **84**, 155440 (2011).

[5] H. K. Pal, V. I. Yudson, and D. L. Maslov, Effect of electron-electron interaction on surface transport in the Bi_2Te_3 family of three-dimensional topological insulators, Phys. Rev. B **85**, 085439 (2012).

[6] Z. B. Siu, M. B. A. Jalil, and S. G. Tan, Topological state transport in topological insulators under the influence of hexagonal warping and exchange coupling to in-plane magnetizations, Sci. Rep. **4**, 5062 (2014).

[7] E. V. Repin and I. S. Burmistrov, Surface states in a 3D topological insulator: The role of hexagonal warping and curvature, J. Exp. Theor. Phys. **121**, 509 (2015).

[8] R. S. Akzyanov and A. L. Rakhmanov, Surface charge conductivity of a topological insulator in a magnetic field: The effect of hexagonal warping, Phys. Rev. B **97**, 075421 (2018).

[9] J. Sinova, S. O. Valenzuela, J. Wunderlich, C. Back, and T. Jungwirth, Spin Hall effects, Rev. Mod. Phys. **87**, 1213 (2015).

[10] J. Sinova, D. Culcer, Q. Niu, N. A. Sinitsyn, T. Jungwirth, and A. H. MacDonald, Universal Intrinsic Spin Hall Effect, Phys. Rev. Lett. **92**, 126603 (2004).

[11] S. Murakami, N. Nagaosa, and S.-C. Zhang, Dissipationless quantum spin current at room temperature, Science **301**, 1348 (2003).

[12] J.-i. Inoue, G. E. W. Bauer, and L. W. Molenkamp, Suppression of the persistent spin Hall current by defect scattering, Phys. Rev. B **70**, 041303 (2004).

[13] R. Raimondi and P. Schwab, Spin-Hall effect in a disordered two-dimensional electron system, Phys. Rev. B **71**, 033311 (2005).

[14] D. Ralph and M. Stiles, Spin transfer torques, J. Magn. Magn. Mater. **320**, 1190 (2008).

[15] W. Chen, M. Sigrist, J. Sinova, and D. Manske, Minimal Model of Spin-Transfer Torque and Spin Pumping Caused by the Spin Hall Effect, Phys. Rev. Lett. **115**, 217203 (2015).

[16] K. L. Wang, J. G. Alzate, and P. K. Amiri, Low-power non-volatile spintronic memory: STT-RAM and beyond, J. Phys. D: Appl. Phys. **46**, 074003 (2013).

[17] A. R. Mellnik, J. S. Lee, A. Richardella, J. L. Grab, P. J. Mintun, M. H. Fischer, A. Vaezi, A. Manchon, E.-A. Kim, N. Samarth *et al.*, Spin-transfer torque generated by a topological insulator, Nature (London) **511**, 449 (2014).

[18] Y. Fan, P. Upadhyaya, X. Kou, M. Lang, S. Takei, Z. Wang, J. Tang, L. He, L.-T. Chang, M. Montazeri *et al.*, Magnetization switching through giant spin-orbit torque in a magnetically doped topological insulator heterostructure, Nature Mater. **13**, 699 (2014).

[19] Y. Fan, X. Kou, P. Upadhyaya, Q. Shao, L. Pan, M. Lang, X. Che, J. Tang, M. Montazeri, K. Murata *et al.*, Electric-field control of spin-orbit torque in a magnetically doped topological insulator, Nature Nano **11**, 352 (2016).

[20] J. Han, A. Richardella, S. A. Siddiqui, J. Finley, N. Samarth, and L. Liu, Room-Temperature Spin-Orbit Torque Switching Induced by a Topological Insulator, Phys. Rev. Lett. **119**, 077702 (2017).

[21] F. Yang, S. Ghatak, A. A. Taskin, K. Segawa, Y. Ando, M. Shiraishi, Y. Kanai, K. Matsumoto, A. Rosch, and Y. Ando, Switching of charge-current-induced spin polarization in the topological insulator $BiSbTeSe_2$, Phys. Rev. B **94**, 075304 (2016).

[22] K. Kondou, R. Yoshimi, A. Tsukazaki, Y. Fukuma, J. Matsuno, K. S. Takahashi, M. Kawasaki, Y. Tokura, and Y. Otani, Fermi-level-dependent charge-to-spin current conversion by Dirac surface states of topological insulators, Nature Phys. **12**, 1027 (2016).

[23] Y. Shiomi, K. Nomura, Y. Kajiwara, K. Eto, M. Novak, K. Segawa, Y. Ando, and E. Saitoh, Spin-Electricity Conversion Induced by Spin Injection into Topological Insulators, Phys. Rev. Lett. **113**, 196601 (2014).

[24] Y. Wang, P. Deorani, K. Banerjee, N. Koirala, M. Brahlek, S. Oh, and H. Yang, Topological Surface States Originated Spin-Orbit Torques in Bi_2Se_3, Phys. Rev. Lett. **114**, 257202 (2015).

[25] H. Wang, J. Kally, J. S. Lee, T. Liu, H. Chang, D. R. Hickey, K. A. Mkhoyan, M. Wu, A. Richardella, and N. Samarth, Surface-State-Dominated Spin-Charge Current Conversion in Topological-Insulator–Ferromagnetic-Insulator Heterostructures, Phys. Rev. Lett. **117**, 076601 (2016).

[26] M. Jamali, J. S. Lee, J. S. Jeong, F. Mahfouzi, Y. Lv, Z. Zhao, B. K. Nikolić, K. A. Mkhoyan, N. Samarth, and J.-P. Wang, Giant spin pumping and inverse spin hall effect in the presence of surface and bulk spin-orbit coupling of topological insulator Bi_2Se_3, Nano Lett. **15**, 7126 (2015).

[27] P. B. Ndiaye, C. A. Akosa, M. H. Fischer, A. Vaezi, E.-A. Kim, and A. Manchon, Dirac spin-orbit torques and charge pumping at the surface of topological insulators, Phys. Rev. B **96**, 014408 (2017).

[28] K. Yasuda, A. Tsukazaki, R. Yoshimi, K. S. Takahashi, M. Kawasaki, and Y. Tokura, Large Unidirectional Magnetoresistance in a Magnetic Topological Insulator, Phys. Rev. Lett. **117**, 127202 (2016).

[29] P. He, S. S.-L. Zhang, D. Zhu, Y. Liu, Y. Wang, J. Yu, G. Vignale, and H. Yang, Bilinear magnetoelectric resistance as a probe of three-dimensional spin texture in topological surface states, Nature Phys. **14**, 495 (2018).

[30] S. S.-L. Zhang and G. Vignale, Theory of bilinear magnetoelectric resistance from topological-insulator surface states, Proc. SPIE **10732**, 1073215 (2018).

[31] K. Yasuda, A. Tsukazaki, R. Yoshimi, K. Kondou, K. S. Takahashi, Y. Otani, M. Kawasaki, and Y. Tokura, Current-Nonlinear Hall Effect and Spin-Orbit Torque Magnetization Switching in a Magnetic Topological Insulator, Phys. Rev. Lett. **119**, 137204 (2017).

[32] M.-F. Yang and M.-C. Chang, Středa-like formula in the spin Hall effect, Phys. Rev. B **73**, 073304 (2006).

[33] D. Kodderitzsch, K. Chadova, and H. Ebert, Linear response Kubo-Bastin formalism with application to the anomalous and spin Hall effects: A first-principles approach, Phys. Rev. B **92**, 184415 (2015).

[34] C. Sahin and M. E. Flatte, Tunable Giant Spin Hall Conductivities in a Strong Spin-Orbit Semimetal: $Bi_{1-x}Sb_x$, Phys. Rev. Lett. **114**, 107201 (2015).

[35] X. Peng, Y. Yang, R. R. Singh, S. Y. Savrasov, and D. Yu, Spin generation via bulk spin current in three-dimensional topological insulators, Nature Commun. **7**, 10878 (2016).

[36] N. A. Sinitsyn, J. E. Hill, H. Min, J. Sinova, and A. H. MacDonald, Charge and Spin Hall Conductivity in Metallic Graphene, Phys. Rev. Lett. **97**, 106804 (2006).

[37] Z. Liu, M. Zhu, and Y. Zheng, Quantum transport properties of graphene in the presence of randomly distributed spin-orbit coupling impurities, Phys. Rev. B **92**, 245438 (2015).

[38] J. H. Garcia and T. G. Rappoport, Kubo-Bastin approach for the spin Hall conductivity of decorated graphene, 2D Mater. **3**, 024007 (2016).

[39] Y. Sun, Y. Zhang, C. Felser, and B. Yan, Strong Intrinsic Spin Hall Effect in the TaAs Family of Weyl Semimetals, Phys. Rev. Lett. **117**, 146403 (2016).

[40] C.-X. Liu, X.-L. Qi, H. Zhang, X. Dai, Z. Fang, and S.-C. Zhang, Model Hamiltonian for topological insulators, Phys. Rev. B **82**, 045122 (2010).

[41] Y. Kohsaka, T. Machida, K. Iwaya, M. Kanou, T. Hanaguri, and T. Sasagawa, Spin-orbit scattering visualized in quasiparticle interference, Phys. Rev. B **95**, 115307 (2017).

[42] N. A. Sinitsyn, E. M. Hankiewicz, W. Teizer, and J. Sinova, Spin Hall and spin-diagonal conductivity in the presence of Rashba and Dresselhaus spin-orbit coupling, Phys. Rev. B **70**, 081312 (2004).

[43] N. Shon and T. Ando, Quantum transport in two-dimensional graphite system, J. Phys. Soc. Jpn. **67**, 2421 (1998).

[44] T. Kato, Y. Ishikawa, H. Itoh, and J.-i. Inoue, Anomalous Hall effect in spin-polarized two-dimensional electron gases with Rashba spin-orbit interaction, New J. Phys. **9**, 350 (2007).

[45] B. Y.-K. Hu, E. H. Hwang, and S. Das Sarma, Density of states of disordered graphene, Phys. Rev. B **78**, 165411 (2008).

[46] T. Chiba, S. Takahashi, and G. E. W. Bauer, Magnetic-proximity-induced magnetoresistance on topological insulators, Phys. Rev. B **95**, 094428 (2017).

[47] P. Adroguer, D. Carpentier, J. Cayssol, and E. Orignac, Diffusion at the surface of topological insulators, New J. Phys. **14**, 103027 (2012).

[48] C. Chen, Z. Xie, Y. Feng, H. Yi, A. Liang, S. He, D. Mou, J. He, Y. Peng, X. Liu *et al.*, Tunable dirac fermion dynamics in topological insulators, Sci. Rep. **3**, 2411 (2013).

[49] P. Cheng, C. Song, T. Zhang, Y. Zhang, Y. Wang, J.-F. Jia, J. Wang, Y. Wang, B.-F. Zhu, X. Chen *et al.*, Landau Quantization of Topological Surface States in Bi_2Se_3, Phys. Rev. Lett. **105**, 076801 (2010).

[50] H. Zhang, C.-X. Liu, X.-L. Qi, X. Dai, Z. Fang, and S.-C. Zhang, Topological insulators in Bi_2Se_3, Bi_2Te_3, and Sb_2Te_3 with a single Dirac cone on the surface, Nature Phys. **5**, 438 (2009).

[51] A. Wolos, S. Szyszko, A. Drabinska, M. Kaminska, S. G. Strzelecka, A. Hruban, A. Materna, and M. Piersa, Landau-Level Spectroscopy of Relativistic Fermions with Low Fermi Velocity in the Bi_2Te_3 Three-Dimensional Topological Insulator, Phys. Rev. Lett. **109**, 247604 (2012).

[52] M. Sakano, M. S. Bahramy, A. Katayama, T. Shimojima, H. Murakawa, Y. Kaneko, W. Malaeb, S. Shin, K. Ono, H. Kumigashira *et al.*, Strongly Spin-Orbit Coupled Two-Dimensional Electron Gas Emerging near the Surface of Polar Semiconductors, Phys. Rev. Lett. **110**, 107204 (2013).

[53] B. A. Piot, W. Desrat, D. K. Maude, M. Orlita, M. Potemski, G. Martinez, and Y. S. Hor, Hole Fermi surface in Bi_2Se_3 probed by quantum oscillations, Phys. Rev. B **93**, 155206 (2016).

[54] M. Nomura, S. Souma, A. Takayama, T. Sato, T. Takahashi, K. Eto, K. Segawa, and Y. Ando, Relationship between Fermi surface warping and out-of-plane spin polarization in topological insulators: A view from spin- and angle-resolved photoemission, Phys. Rev. B **89**, 045134 (2014).

[55] P. Rakyta, A. Pályi, and J. Cserti, Electronic standing waves on the surface of the topological insulator Bi_2Te_3, Phys. Rev. B **86**, 085456 (2012).

[56] N. H. D. Khang, Y. Ueda, and P. N. Hai, A conductive topological insulator with large spin Hall effect for ultralow power spin-orbit torque switching, Nature Mater. **17**, 808 (2018).

[57] S. Singh, A. C. Garcia-Castro, I. Valencia-Jaime, F. Muñoz, and A. H. Romero, Prediction and control of spin polarization in a Weyl semimetallic phase of BiSb, Phys. Rev. B **94**, 161116 (2016).

[58] M. S. Bahramy, R. Arita, and N. Nagaosa, Origin of giant bulk Rashba splitting: Application to BiTeI, Phys. Rev. B **84**, 041202(R) (2011).

[59] P. D. C. King, R. C. Hatch, M. Bianchi, R. Ovsyannikov, C. Lupulescu, G. Landolt, B. Slomski, J. H. Dil, D. Guan, J. L. Mi *et al.*, Large Tunable Rashba Spin Splitting of a Two-Dimensional Electron Gas in Bi_2Se_3, Phys. Rev. Lett. **107**, 096802 (2011).

[60] B. Habib, J. Shabani, E. P. De Poortere, M. Shayegan, and R. Winkler, Tuning of the spin-orbit interaction in two-dimensional GaAs holes via strain, Phys. Rev. B **75**, 153304 (2007).

[61] T. Förster, P. Krüger, and M. Rohlfing, *GW* calculations for Bi_2Te_3 and Sb_2Te_3 thin films: Electronic and topological properties, Phys. Rev. B **93**, 205442 (2016).

[62] R. S. Akzyanov, Thin film of a topological insulator as a spin Hall insulator, arXiv:1807.04611.

[63] D. Culcer, A. Sekine, and A. H. MacDonald, Interband coherence response to electric fields in crystals: Berry-phase contributions and disorder effects, Phys. Rev. B **96**, 035106 (2017).

[64] D. Culcer, M. E. Lucassen, R. A. Duine, and R. Winkler, Current-induced spin torques in III-V ferromagnetic semiconductors, Phys. Rev. B **79**, 155208 (2009).